

Magnetic Field Calculation for Flat Permanent-Magnet Linear Machines Using a Hybrid Analytical Model

Brahim Ladghem-Chikouche, Kamel Boughrara, Frédéric Dubas, Lazhar Roubache, and Rachid Ibtouen

Abstract—This paper proposes an improved two-dimensional (2-D) hybrid analytical method (HAM) in Cartesian coordinates, based on the exact subdomain (SD) technique and the finite-difference method (FDM). It is applied to flat permanent-magnet (PM) linear machines with dual-rotor. The magnetic field solution is obtained by coupling an exact SD model, calculated in all regions having relative permeability equal to unity, with FDM in ferromagnetic regions. The analytical model and FDM are connected in both axes (x, y) of the (non-)periodicity direction (i.e., in the interface between the tooth regions and all its adjacent regions as slots and/or air-gap). To provide accuracy solutions, the current density distribution in slot regions is modeled by using Maxwell's equations. It is found that, whatever the iron core magnetic parameters, the developed HAM gives accurate results for no- and on-load conditions. Finite-element analysis (FEA) demonstrates excellent results of the developed technique.

Keywords— Hybrid magnetic model, exact subdomain technique, finite difference method, finite-element analysis.

I. INTRODUCTION

Flat PM linear machines with dual-rotor present many important industrial applications due to their multiple advantages compared to conventional machines, namely: compactness, high-torque density, precise control, and dynamic performance.

Recently, several design models have been proposed and developed for these machines in view to introduce the nonlinearity of the $B(H)$ curve into the analytical solution, such as the analytical approach (e.g., based on the exact SD technique) or/and the HAM. The latter has become important and is preferred for different reasons, such as the accuracy, the saturation effect, and the computation time.

One of the critical deficiencies of the different published methods and techniques concerns the magnetic characteristic of ferromagnetic core, when the authors, to facilitate their calculations, suppose that the iron core relative permeability is equal to infinity. This problem has been solved by different technique such as the HAM which has been proposed by different techniques:

- i. In [1]-[2], a coupling between the Maxwell-Fourier methods and FEA is achieved via the boundary integral

Manuscript received May 5, 2021; revised July 26, 2021.

Brahim Ladghem-Chikouche is with the Department of Electrical Engineering, Faculty of Technology, University of M'sila, Algeria and with Laboratoire de Recherche en Electrotechnique (LRE-ENP), Ecole Nationale Polytechnique, Algeria (e-mail: brahim.lch@univ-m'sila.dz).

Kamel Boughrara, and Rachid Ibtouen are with LRE-ENP, Ecole Nationale Polytechnique, (e-mail: kamel.boughrara@g.enp.edu.dz, rachid.ibtiouen@gmail.com).

Frédéric Dubas is with Département ENERGIE, FEMTO-ST, CNRS, Univ. Bourgogne Franche-Comté, F90000 Belfort, France (e-mail: fdubas@gmail.com).

Lazhar Roubache is with the Department of Electrical Engineering, Faculty of Technology, University of M'sila, Algeria (e-mail: roubache.lazhar@gmail.com).

Digital Object Identifier (DOI): 10.53907/enpesj.v1i2.36

- term in the air-gap region. The proposed method eliminates the need for finite-elements in the air-gap. In [2], the saturation effect is considered.
- ii. In [3]-[12], a coupling between the Maxwell-Fourier methods and the magnetic equivalent circuit (MEC) are presented for no- and on-load conditions. In [3], the magnetic potential drop can be replaced by equivalent current sheets in the slots in order to represent the nonlinearity magnetostatic effect for loaded conditions. The hybrid method is used for the analysis of axial or radial flux rotating or tubular linear machines. Some of them can consider the saturation effect on the exact SD technique. The armature winding currents is represented by equivalent magneto-motive force (MMF).
- iii. Improved conformal mapping coupled with MEC is presented in [13]-[16]. This technique has been validated for any complex stator. It is suitable for machines with small number of slots per pole and phase.
- iv. In [17]-[18], a direct coupling between FEA and MEC is proposed. However, in [18], the proposed MEC is used to predict the no-load characteristics firstly and then the proposed 2-D equivalent FEA is used to predict the load characteristics at the preliminary design stage.
- v. In [19]-[22], a coupling between FDM and FEA is developed.
- vi. The electromagnetic performances are calculated by means of a 2-D HAM combining the SD technique and FDM [23]-[24].

This paper deals with new HAM based on the Maxwell-Fourier methods, based on the exact SD technique, and FDM. It covers comprehensively any modeling related to a complex electromagnetic device. In this paper, the HAM is applied to flat PM linear machines with dual-rotor. The main contribution is to establish a direct coupling between the SD technique and numerical method based on the finite-difference in the interface separating the iron core and the vacuum. In order to accurately predict the electromagnetic performances, a direct coupling is assumed in both directions

(x - and y -edges) considering the finite permeability of the ferromagnetic core.

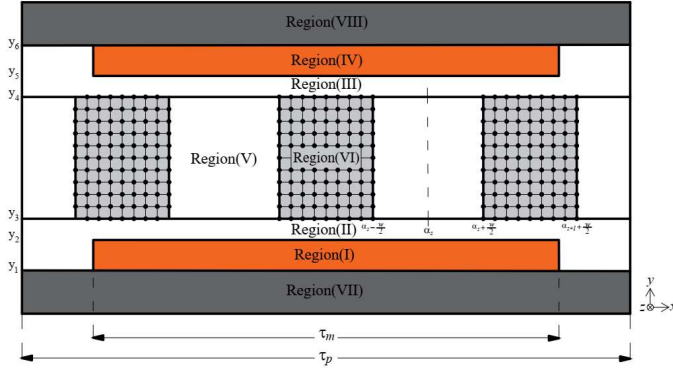


Fig. 1: Proposed flat linear PM synchronous machine with dual-rotor having a radial magnetization and a single-layer concentrated winding.

TABLE I
MACHINE CHARACTERISTICS

Symbol	Parameter (unit)	Value
B_{rm}	Remanent of flux density of PMs (T)	1.25
-	Magnetization type	Radial
Q	Number of stator slots per pole	3
y_1	Inner magnet height (mm)	7
y_2	Outer magnet height (mm)	12
y_3	Inner slot height (mm)	12.5
y_4	Outer slot height (mm)	27.5
y_5	Outer magnet height (mm)	28
y_6	Inner magnet height (mm)	33
y_7	Outer yoke height (mm)	40
β	PM pole-width to pole-pitch ratio	100%
w	Slot opening width (mm)	12
τ_p	Pole pitch (mm)	60
J_m	Armature current density (A/m^2)	$15 \cdot 10^6$
L	Axial length (mm)	50
nh	Harmonics number	140

To evaluate the efficacy of the proposed HAM, the magnetic flux density distribution in the whole electromagnetic device was compared with those obtained by the 2-D FEA [25]. FEA demonstrates highly accurate results of the developed technique. The 2-D HAM is ≈ 2 times faster than 2-D FEA with high accuracy.

II. PROBLEM DESCRIPTION AND ASSUMPTIONS

The proposed flat PM linear synchronous machine with rotordual is depicted in Fig. 1. The main geometrical and physical parameters are listed in Table I. This machine is composed of:

- PMs: Region I and IV;
- Vacuum: Region II and III;
- Q slots with coils: Region V;
- Q teeth: Region VI;
- Iron yokes: Region VII and VIII.

The rotor topology is constituted of multi-poles PMs mounted on the rotor surface with a radial magnetization. The moving PMs can have a more diversity of magnetization. The stator slots topology is proposed with a radial-sided surface. The spatial distribution of 3-phases winding is configured in a standard manner with a single-layer in the slot (i.e., non-

overlapping or concentrated winding).

In the 2-D cartesian coordinate system, some assumptions are made in this paper to limit the mathematical efforts, as in [26]-[27].

III. FORMULATION OF HAM

A. Introduction

In this paper, a 2-D HAM based on the SD technique and FDM is presented. Each SD of the proposed machine is modeled under fixed absolute permeability $\mu = C^{st}$. The SDs are expressed by a partial differential equation (PDE) in terms of \mathbf{A} [27].

$$\nabla^2 \mathbf{A} = -[\mu \mathbf{J} + \mu_0 \nabla \times \mathbf{Mr}] \quad (1)$$

where \mathbf{J} is the current density (due to supply currents) vector, \mathbf{Mr} is the remanent magnetization vector (with $\mathbf{Mr} = 0$ for the vacuum/iron or $\mathbf{Mr} \neq 0$ for the PMs according to the magnetization direction), and $\mu = \mu_0 \mu_r$ is the absolute magnetic permeability of the magnetic material in which μ_0 and μ_r are respectively the vacuum permeability and the relative permeability of the magnetic material (with $\mu_r = 1$ for the vacuum or $\mu_r \neq 1$ for the PMs/iron).

B. 2-D Exact SD Technique

From Equation (1), the general PDEs in terms of \mathbf{A} in the Region I to V can be written as:

$$\nabla^2 \mathbf{A} = -\mu_0 \nabla \times \mathbf{Mr} \quad \text{in Region I and IV} \quad (2a)$$

$$\nabla^2 \mathbf{A} = 0 \quad \text{in Region II and III} \quad (2b)$$

$$\nabla^2 \mathbf{A} = -\mu_0 \mathbf{J} \quad \text{in Region V} \quad (2c)$$

The remanent magnetization vector of PMs can be expressed by

$$\mathbf{Mr} = Mr_x \mathbf{u}_x + Mr_y \mathbf{u}_y \quad (3)$$

where Mr_x and Mr_y are respectively the x - and y -component of \mathbf{Mr} .

The field vectors $\mathbf{B} = \{B_x; B_y; 0\}$ and $\mathbf{H} = \{H_x; H_y; 0\}$ are coupled by the magnetic material equation

$$\mathbf{B} = \mu_m \mathbf{H} + \mu_0 \mathbf{Mr} \quad \text{in Region I and IV} \quad (4)$$

$$\mathbf{B} = \mu_0 \mathbf{H} \quad \text{in other regions} \quad (5)$$

Using $\mathbf{B} = \nabla \times \mathbf{A}$, the components of \mathbf{B} can be deduced by

$$B_x = \frac{\partial A_z}{\partial y} \quad \& \quad B_y = -\frac{\partial A_z}{\partial x} \quad (6)$$

In Cartesian coordinates (x, y) , Equation (2) in terms of $\mathbf{A} = \{0; 0; A_z\}$ can be rewritten as

- in Region I and IV (i.e., Poisson's equation):

$$\frac{\partial^2 A_z^{I,IV}}{\partial x^2} + \frac{\partial^2 A_z^{I,IV}}{\partial y^2} = -\mu_0 \cdot \left(\frac{\partial Mr_y}{\partial x} - \frac{\partial Mr_x}{\partial y} \right) \quad (7)$$

- in Region II and III (i.e., Laplace's equation):

$$\frac{\partial^2 A_z^{II,III}}{\partial x^2} + \frac{\partial^2 A_z^{II,III}}{\partial y^2} = 0 \quad (8)$$

- in Region V (i.e., Poisson's equation):

$$\frac{\partial^2 A_z^V}{\partial x^2} + \frac{\partial^2 A_z^V}{\partial y^2} = -\mu_0 \cdot J_z \quad (9)$$

In order to obtain the solution of Laplace's and Poisson

equations in different regions, the PDEs (7) ~ (9) can be solved by using the separation of variables method and the Dubas' superposition technique [27]. All regions of the proposed machine are described by Fourier series expression in both directions (i.e., x - and y -edges). Hence, the general solution of A_z , in SDs is the superposition of two components in x - and y -directions [26]-[27]:

- in Region I and IV:

$$A_z^{I,IV} = \sum_n \left(C_{3n}^{I,IV} \cdot e^{K_n y} + C_{4n}^{I,IV} \cdot e^{-K_n y} + \Gamma_s \right) \cdot \sin(K_n x) + \sum_n \left(C_{5n}^{I,IV} \cdot e^{K_n y} + C_{6n}^{I,IV} \cdot e^{-K_n y} + \Gamma_c \right) \cdot \cos(K_n x) \quad (10a)$$

where

$$K_n = \frac{\pi n}{\tau_p}, \quad \Gamma_s = -\mu_o \cdot \frac{Mr_{ycn}}{K_n}, \quad \Gamma_c = \mu_o \cdot \frac{Mr_{ysn}}{K_n} \quad (10b)$$

τ_p is the pole pitch.

- in Region II and III:

$$A_z^{II,III} = \sum_n \left(C_{3n}^{II,III} \cdot e^{K_n y} + C_{4n}^{II,III} \cdot e^{-K_n y} \right) \cdot \sin(K_n x) + \sum_n \left(C_{5n}^{II,III} \cdot e^{K_n y} + C_{6n}^{II,III} \cdot e^{-K_n y} \right) \cdot \cos(K_n x) \quad (11)$$

- in Region V:

$$A_{zs}^V = C_{s1}^V + C_{s2}^V \cdot y - \frac{1}{2} \cdot \mu_o \cdot J_{zs} \cdot y^2 + \sum_m G_{sm}^{Vx} \cdot \cos \left[\beta_m^V \cdot \left(x - \alpha_s + \frac{w}{2} \right) \right] + \sum_v G_{sv}^{Vy} \cdot \sin \left[\lambda_v^V \cdot (y - y_3) \right] \quad (12a)$$

$$G_{sm}^{Vx} = C_{s3m}^V \cdot e^{\beta_m^V y} + C_{s4m}^V \cdot e^{-\beta_m^V y} \quad (12b)$$

$$G_{sv}^{Vy} = C_{s5v}^V \cdot \sinh \left[\lambda_v^V \cdot \left(x - \alpha_s + \frac{w}{2} \right) \right] + C_{s6v}^V \cdot \sinh \left[\lambda_v^V \cdot \left(x - \alpha_s - \frac{w}{2} \right) \right] \quad (12c)$$

with

$$J_{zs} = J_m \cdot [1 \ 1 \ 0 \ -1 \ -1 \ 0 \ 1 \ 1 \ 0 \ -1 \ -1 \ 0] \quad (13)$$

where J_m is the current density peak, w is the slot-opening, α_s is the position of s^{th} slot, m and v are the spatial harmonic orders, β_m^V and λ_v^V are the spatial frequency (or periodicity) in both directions defined by:

$$\beta_m^V = \frac{m\pi}{w} \quad \& \quad \lambda_v^V = \frac{v\pi}{y_4 - y_3} \quad (14)$$

C. 2-D FDM

In Region VI, the solution of magnetic vector potential distribution can be achieved from numerical Maxwell's equations. According to Fig. 2, the grill nodes located in the ferromagnetic region is obtained with a uniform mesh. The magnetic flux can be written as:

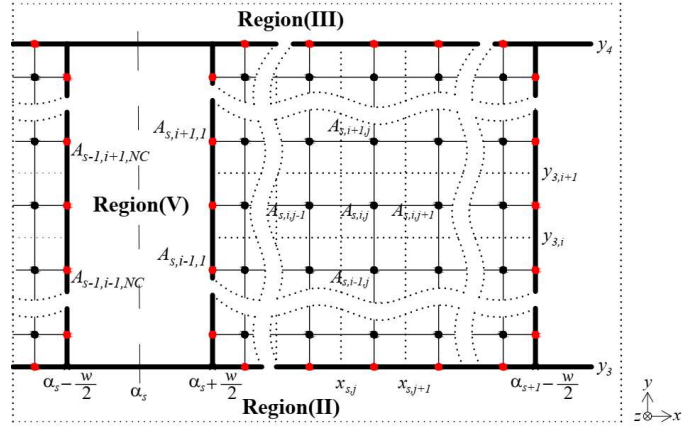


Fig. 2: Uniform mesh of the Region VI discretized into several nodes

$$\frac{\Delta^2 A_z^{VI}}{\Delta x^2} + \frac{\Delta^2 A_z^{VI}}{\Delta y^2} = 0 \quad (15)$$

Equation (6) should be rewritten using numerical differentiation defined as the limit of a difference quotient as:

$$B_x(x) = \lim_{\Delta x \rightarrow 0} \left(\frac{\Delta A}{\Delta x} \right) \quad \& \quad B_y(y) = \lim_{\Delta y \rightarrow 0} \left(-\frac{\Delta A}{\Delta y} \right) \quad (16)$$

The difference quotient $B_x(x)$ and $B_y(y)$ is a derivative approximation. This improves as Δx and Δy become smaller. Δx and Δy are the spacing between two adjacent nodes in the x - and y -direction, respectively

$$\Delta x = x_{s,j+1} - x_{s,j} \quad (17a)$$

$$\Delta y = y_{3,i+1} - y_{3,i} \quad (17b)$$

According to Equation (15) and Fig. 2, each term of the PDE at the particular node is replaced by a finite-difference approximation. The distribution of A_z in the Region VI can be rewritten as:

$$\frac{A_{zs,i,j+1}^{VI} - 2A_{zs,i,j}^{VI} + A_{zs,i,j-1}^{VI}}{\Delta x^2} + \frac{A_{zs,i+1,j}^{VI} - 2A_{zs,i,j}^{VI} + A_{zs,i-1,j}^{VI}}{\Delta y^2} = 0 \quad (18)$$

IV. BOUNDARY AND INTERFACE CONDITIONS

The special feature of this paper is to establish a direct coupling between the two models, especially between regions that do not have the same relative permeability, such as the Region VI and its adjacent regions (namely, II, III and V). For simplicity and to limit the mathematical efforts, the Region VII and VIII are not introduced in the system to be solved. The relative permeability of these regions is supposed to be equal to infinity. It is easy to add these regions in the HAM. For this case and,

- At $y = y_3$ and for the index $s = 1, \dots, Q$:

$$A_{zs,1,j}^{VI} = \frac{1}{\Delta x} \int_{x_{s,j}}^{x_{s,j+1}} A_z^II(x, y) dx \quad (19)$$

$$\left(A_{zs}^V(x, y) = A_z^II(x, y) \right) \Big|_{\alpha_s - \frac{w}{2} \leq x \leq \alpha_s + \frac{w}{2}} \quad (20)$$

$$H_x^II(x, y) = \sum_s \left(\begin{array}{l} H_{xs}^V(x, y) \Big|_{\alpha_s - \frac{w}{2} \leq x \leq \alpha_s + \frac{w}{2}} \\ + H_{xs}^{VI}(x, y) \Big|_{\alpha_s + \frac{w}{2} \leq x \leq \alpha_{s+1} - \frac{w}{2}} \end{array} \right) \quad (21)$$

In order to satisfy Equation (21), the magnetic flux intensity $H_{xs}^{VI}(x, y)$ by applying Equation (16) should be written as:

$$H_{xs}^{VI}(x, y) = \frac{1}{\mu_0 \mu_r} \sum_{j=2}^{Nc-1} \left(\frac{A_{s,2,j}^{VI} - A_{s,1,j}^{VI}}{\Delta y} \right) f_v \quad (22a)$$

$$f_v = \sum_v [h_{xsv}^{VI} \sin(K_n x) + h_{xcv}^{VI} \cos(K_n x)] \quad (22b)$$

where h_{xsv}^{VI} & h_{xcv}^{VI} are the Fourier's constants, and Nc is the number of grid nodes in the x -direction.

- At $y = y_4$ and for the index $s = 1, \dots, Q$:

$$A_{zs,NL,j}^{VI} = \frac{1}{\Delta x} \int_{x_{s,j}}^{x_{s,j+1}} A_z^{III}(x, y) dx \quad (23)$$

$$(A_{zs}^V(x, y) = A_z^{III}(x, y)) \Big|_{\alpha_s - \frac{w}{2} \leq x \leq \alpha_s + \frac{w}{2}} \quad (24)$$

$$H_x^{III}(x, y) = \sum_s \left(\begin{array}{l} H_{xs}^V(x, y) \Big|_{\alpha_s - \frac{w}{2} \leq x \leq \alpha_s + \frac{w}{2}} \\ + H_{xs}^{VI}(x, y) \Big|_{\alpha_s + \frac{w}{2} \leq x \leq \alpha_{s+1} - \frac{w}{2}} \end{array} \right) \quad (25)$$

In order to satisfy Equation (25), the magnetic flux intensity $H_{xs}^{VI}(x, y)$ by applying Equation (16) should be written as:

$$H_{xs}^{VI}(x, y) = \frac{1}{\mu_0 \mu_r} \sum_{j=2}^{Nc-1} \left(\frac{A_{s,NL,j}^{VI} - A_{s,NL-1,j}^{VI}}{\Delta y} \right) f_v \quad (26)$$

On the y -direction, viz., on the edges of the Region V and VI and for the index $s = 1, \dots, Q$:

- for $x = \alpha_s + w/2$:

$$A_{zs,i,1}^{VI} = \frac{1}{\Delta y} \int_{y_{3,i}}^{y_{3,i+1}} A_{zs}^V(x, y) dy \quad (27)$$

$$H_{ys}^{VI}(x, y) = H_{ys}^V(x, y) \quad (28)$$

where

$$H_{ys}^{VI}(x, y) = \frac{1}{\mu_r \mu_0} \sum_{i=2}^{Nl-1} \sum_v \left(-\frac{A_{zs,i,2}^{VI} - A_{zs,i,1}^{VI}}{\Delta x} \right) \cdot h_{ysv}^{VI} \sin[\lambda \cdot (y - y_2)] \quad (29)$$

where Nl is the number of grid nodes in the y -direction and h_{ysv}^{VI} is the Fourier's constants.

For the index $s = 2, \dots, Q$ and,

- for $x = \alpha_s - w/2$:

$$A_{zs,i,Nc}^{VI} = \frac{1}{\Delta y} \int_{y_{3,i}}^{y_{3,i+1}} A_{z(s-1)}^V(x, y) dy \quad (30)$$

$$H_{rs}^{VI}(x, y) = H_{r(s-1)}^V(x, y) \quad (31)$$

where

$$H_{ys}^{VI}(x, y) = \frac{1}{\mu_r \mu_0} \sum_{i=2}^{Nl-1} \sum_v \left(-\frac{A_{zs,i,Nc}^{VI} - A_{zs,i,Nc-1}^{VI}}{\Delta x} \right) \cdot h_{ysv}^{VI} \sin[\lambda \cdot (y - y_2)] \quad (32)$$

Anti-periodic BCs are applied and given as:

$$A_{zQs,i,Nc}^{VI} = -\frac{1}{\Delta y} \int_{y_{3,i}}^{y_{3,i+1}} A_{z1}^V(x, y) dy \quad (33)$$

$$H_{xQs}^{VI}(x, y) = -H_{x1}^V(x, y) \quad (34)$$

V. COMPARISON OF HAM AND NUMERICAL CALCULATIONS

About the FEA, FEMM designer was used, and the analytical calculations were computed by MATLAB. The number of nodes and elements are 84,019 and 167,089, respectively. These results have been calculated under an acceptable amount of discretization of the Region VI (viz., $Nc = 25$ and $Nl = 15$).

Figs. 3 ~ 4 shown a comparison of the air-gap flux density distribution with a radial magnetization pattern and for the open-circuit calculated by HAM and FEA with different values of iron core relative permeability (viz., $\mu_r = 2$ and 1,000) under geometrical and physical parameters given in Table I.

Figs. 5 ~ 6 shown the air-gap magnetic flux density distribution for the armature reaction. The maximal current density is equal to J_m [see Table I].

Excellent agreement is achieved between HAM and FEM.

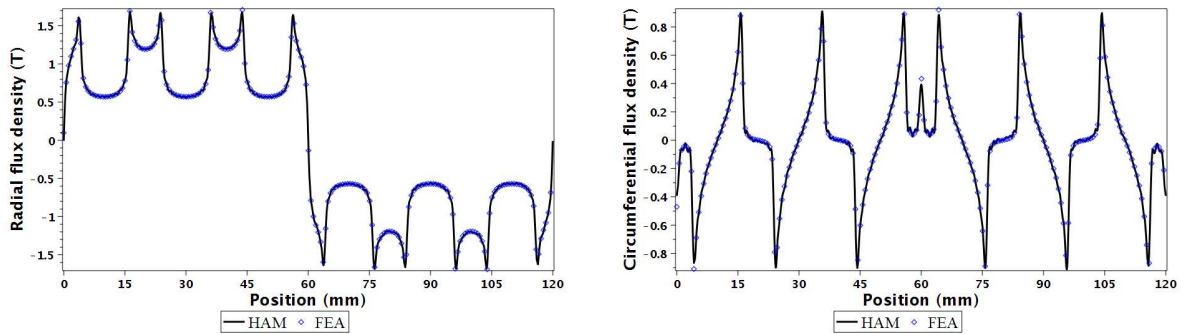


Fig. 3: Comparison of HAM and FEA predicted for the open-circuit magnetic flux density distribution with a radial magnetization pattern in the middle of the Region II for $\mu_r = 1,000$ in all ferromagnetic regions.

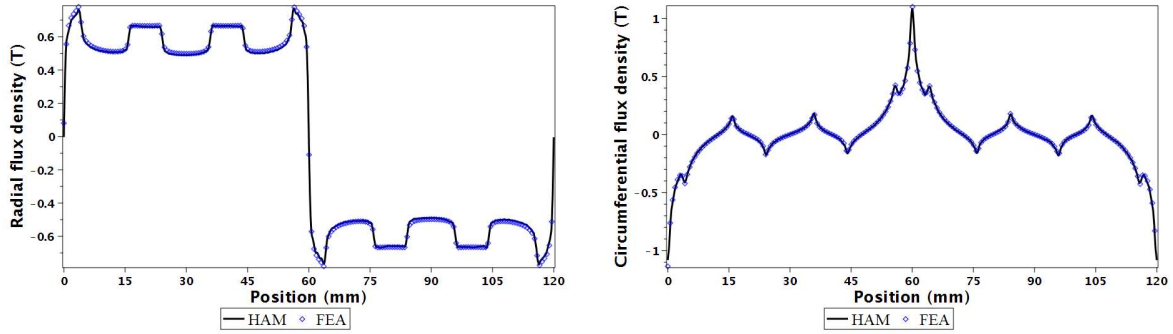


Fig. 4: Comparison of HAM and FEA predicted for the open-circuit magnetic flux density distribution with a radial magnetization pattern in the middle of the Region II for $\mu_r = 2$ in all ferromagnetic regions.

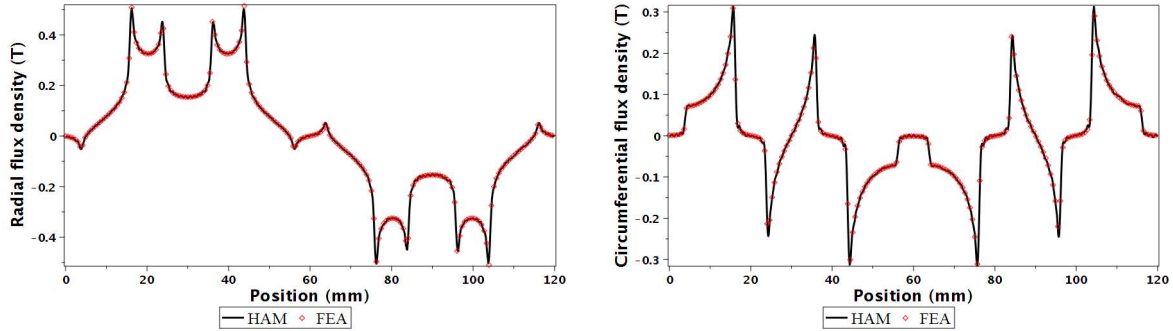


Fig. 5: Comparison of HAM and FEA predicted of the armature reaction magnetic flux density in the middle of the Region II for $\mu_r = 1,000$ in all ferromagnetic regions.

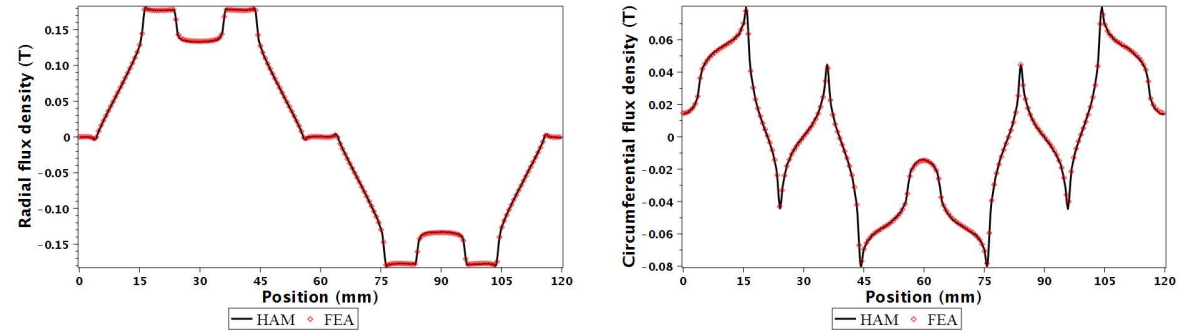


Fig. 6: Comparison of HAM and FEA predicted of the armature reaction magnetic flux density in the middle of the Region II for $\mu_r = 2$ in all ferromagnetic regions.

TABLE II.
2-D COMPUTATIONAL TIME FOR VARIOUS METHODS

Method	HAM	FEA
	$nh = 140$ $Nc = 25, Nl = 15$	Two poles 84,019 nodes
Time (sec)	~3	~7.5

Figs. 7 ~ 10 show the magnetic flux density distribution in all parts of an electrical machine calculated by HAM and compared to FEA with different values of iron core relative permeability (viz., $\mu_r = 2$ and 1,000) as well as the error level calculated by

$$\|B_{error}\| = \frac{\| \|B_{FEA}\| - \|B_{HAM}\| \|}{\text{mean}(\|B_{FEA}\|)} \times 100\% \quad (35)$$

Each SDs of the proposed machine is divided into 50 levels in the y -direction and each level is composed to 1,200 points in the x -direction. We can observe that the errors can be localized in the interface between two adjacent regions or in the edges of PMs and that because of the fluctuations due to limiting number of Fourier series harmonics.

Table II shown the computation time for the magnetic flux density calculation by HAM and FEA.

VI. CONCLUSION

This paper presents a new HAM based on an accurate SD model and FDM for the flat PM linear synchronous machine with rotor-dual having a radial magnetization and a single-layer concentrated winding. The proposed approach is modeled in 2-D Cartesian coordinates using Maxwell's equations. The coupling between the two models is performed especially in the interface when two adjacent regions have not the same magnetic parameters (e.g., in the interface between teeth regions and all its adjacent regions). It was performed in both directions (x - and y -edges) in order to gives accurate results, especially in case of saturation effect.

The HAM was used to predict the magnetic flux density components whatever the loading conditions (i.e., the open-circuit and the armature reaction) and the iron core relative permeability. The comparison with 2-D FEA demonstrates excellent results of the developed approach. The computational time is ≈ 2 times smaller than FEA.

The high impact contributions of this approach can now focus our attention on the optimization of the machine performances, in particular with the local saturation effect through elementary SD technique [28] by inserting the $B(H)$ curve which will be proposed in a future contribution.

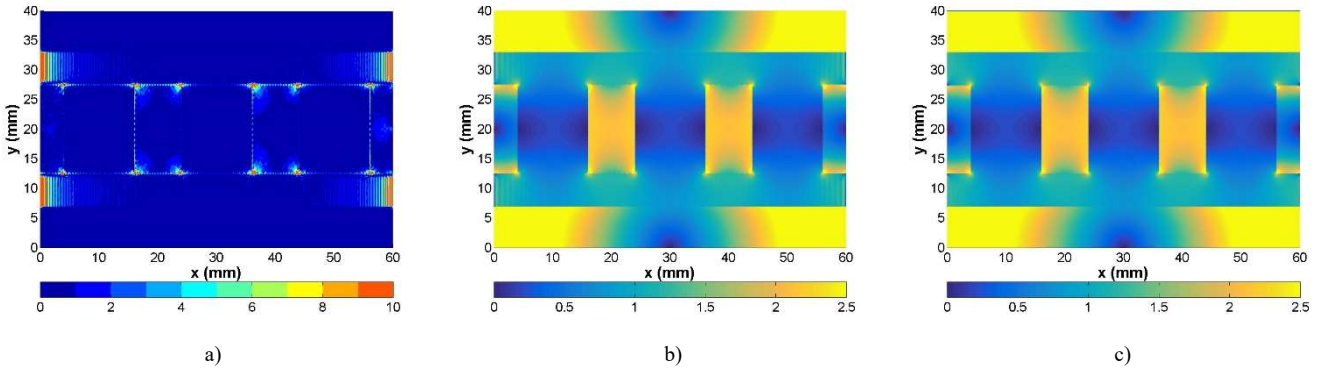


Fig. 7: a) $\|B_{error}\|(\%)$ distribution calculated by the difference between b) HAM and c) FEA under no-load condition for $\mu_r = 1,000$.

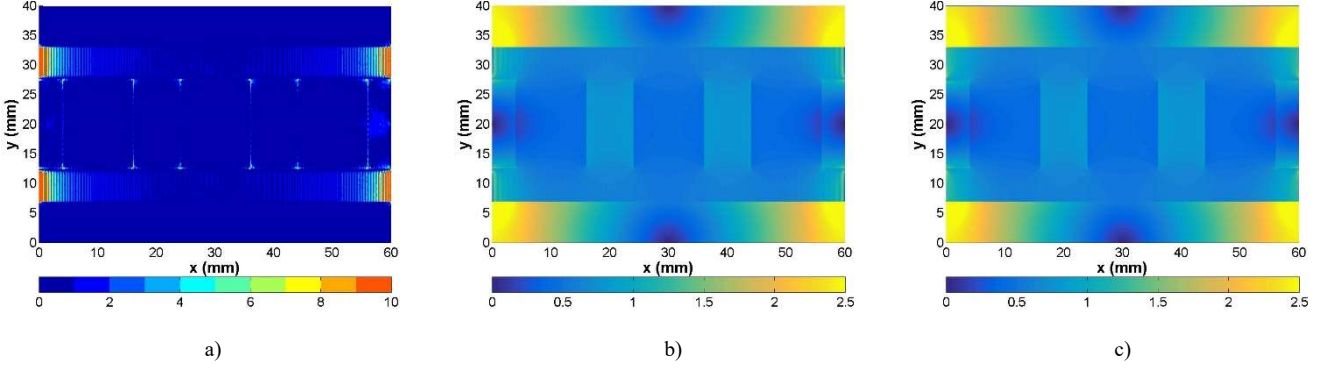


Fig. 8: a) $\|B_{error}\|(\%)$ distribution calculated by the difference between b) HAM and c) FEA under no-load condition for $\mu_r = 2$.

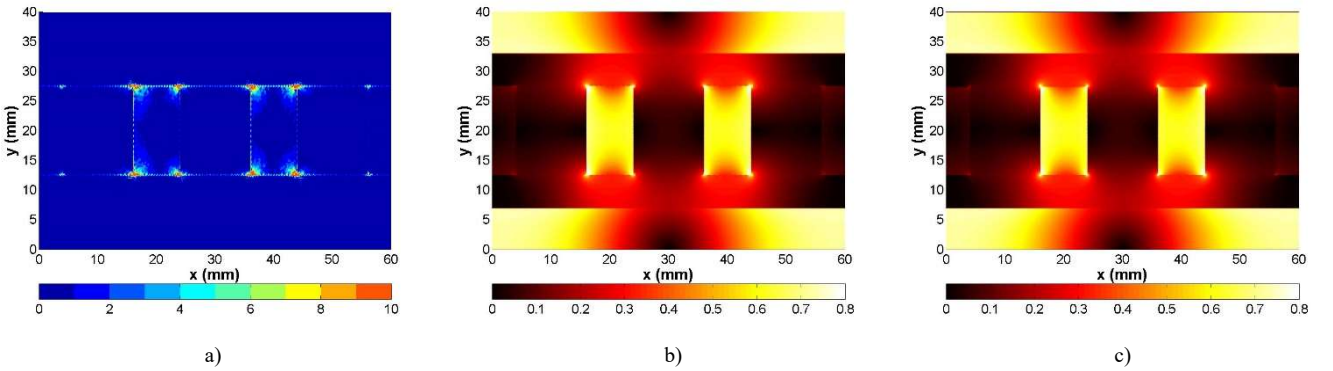


Fig. 9: a) $\|B_{error}\|(\%)$ distribution calculated by the difference between b) HAM and c) FEA under armature reaction condition for $\mu_r = 1,000$.

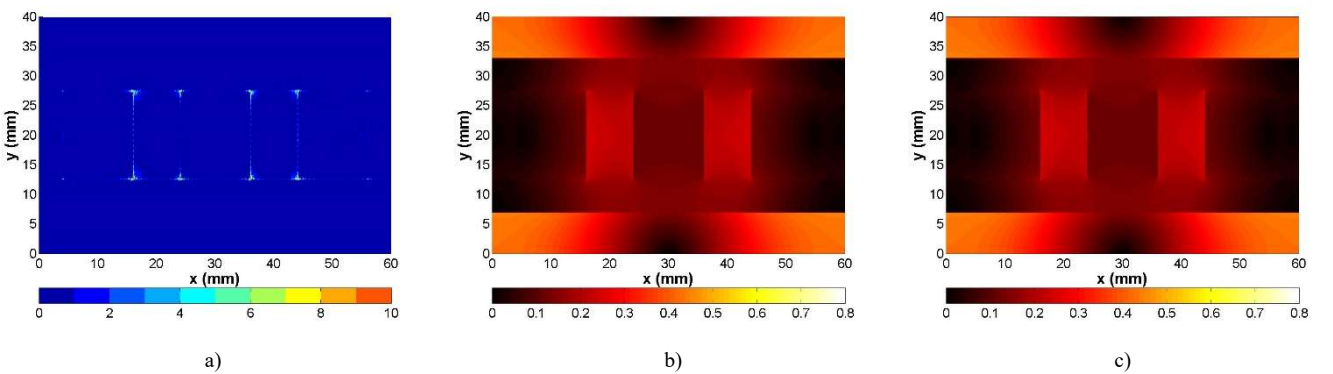


Fig. 10: a) $\|B_{error}\|(\%)$ distribution calculated by the difference between b) HAM and c) FEA under armature reaction condition for $\mu_r = 2$.

ACKNOWLEDGMENT

The authors acknowledge the financial support of the General Directorate of Scientific Research and Technological Development (DGRSDT) of Algeria.

REFERENCES

- [1] K. Lee, M.J. DeBortoli, M.J. Lee, S.J. Salon, "Coupling Finite Elements and Analytical Solution in the Airgap of Electrical Machines," *IEEE Trans. Magn.*, vol. 27, no. 5, Sep. 1991, pp. 3955-3957, doi: 10.1109/20.104969.
- [2] M. Shen, P-D. Pfister, C. Tang, and Y. Fang, "A hybrid model permanent-magnet machines combining Fourier analytical model with finite element method, taking magnetic saturation into account," *IEEE Trans. Magn.*, vol. 57, no. 2, Feb. 2021, doi: 10.1109/TMAG.2020.3005802.
- [3] L. Wu, H. Yin, D. Wang, and Y. Fang, "On-load field prediction in SPM machines by a subdomain and magnetic circuit hybrid model," *IEEE Trans Ind. Elec.*, vol. 67, no. 9, pp. 7190-7201, Sep. 2020, doi: 10.1109/TIE.2019.2942561.
- [4] H.S. Zhang, Z.X. Deng, M.L. Yang, Y. Zhang, J.Y. Tuo, and J. Xu, "Analytical prediction of Halbach array permanent magnet machines considering finite tooth permeability," *IEEE Trans. Magn.*, vol. 56, no. 6, June 2020, Art. no. 8101010, doi: 10.1109/TMAG.2020.2982844.

- [5] S. Ouagued, Y. Amara, and G. Barakat, "Comparison of hybrid analytical modelling and reluctance network modelling for pre-design purposes," *Mathematics and Computers in Simulation*, vol. 130, pp. 3-21, Dec. 2016, doi: 10.1016/j.matcom.2016.05.001.
- [6] S. Ouagued, Y. Amara, and G. Barakat, "Cogging force analysis of linear permanent magnet machines using a hybrid analytical model," *IEEE Trans. Magn.*, vol. 52, no. 7, July 2016, Art. no. 8202704, doi: 10.1109/TMAG.2016.2521825.
- [7] Y. Benmessaoud, F. Dubas, and M. Hilairt, "Combining the magnetic equivalent circuit and Maxwell-Fourier method for eddy-current loss calculation," *Math. Comput. Appl.*, vol. 24, no. 2, p. 60, June 2019, doi: 10.3390/mca24020060.
- [8] Y. Benmessaoud, D. Ouamara, F. Dubas, and M. Hilairt, "Investigation of volumic permanent-magnet eddy-current losses in multi-phase synchronous machines from hybrid multi-layer model," *Math. Comput. Appl.*, vol. 25, no. 1, p. 14, Mar. 2020, doi: 10.3390/mca25010014.
- [9] D. Ceylan, L.A. J. Friedrich, K.O. Boynov, and E.A. Lomonova, "Convergence analysis of the fixed-point method with the hybrid analytical modeling for 2-D nonlinear magnetostatic problems," *IEEE Trans. Magn.*, Jan. 2021, Art. no. 7500105, doi: 10.1109/TMAG.2020.3024539.
- [10] J. Bao, B.L.J. Gysen, and E.A. Lomonova, "Hybrid analytical modeling of saturated linear and rotary electrical machines: Integration of Fourier modeling and magnetic equivalent circuits," *IEEE Trans. Magn.*, vol. 54, no. 11, Nov. 2018, Art. no. 8109905, doi: 10.1109/TMAG.2018.2837896.
- [11] B. Ladghem-Chikouche, K. Boughrara, F. Dubas, and R. Ibtouen, "Analytical Magnetic Field Calculation for Flat Permanent-Magnet Linear Machines with dual-rotor by using improved 2-D hybrid analytical method", *COMPEL - Int. J. Comput. Math. Electr. Electron. Eng.*, vol. 40, no. 3, pp. 602-623, August, 2021, doi: 10.1108/COMPEL-02-2021-0039.
- [12] B. Ladghem-Chikouche, K. Boughrara, F. Dubas, and R. Ibtouen, "Two-dimensional hybrid model for magnetic field calculation in electrical machines: Exact subdomain technique and magnetic equivalent circuit", *COMPEL - Int. J. Comput. Math. Electr. Electron. Eng.*, vol. 40, no. 3, pp. 535-560, June, 2021, doi: 10.1108/COMPEL-01-2021-0008.
- [13] A. Hanic, D. Zarko, D. Kuhinek, and Z. Hanic, "On-load analysis of saturated surface permanent magnet machines using conformal mapping and magnetic equivalent circuits," *IEEE Trans. Magn.*, vol. 33, no. 3, Sep. 2018, pp. 915-924, doi: 10.1109/TEC.2017.2789322.
- [14] A. Hanic, D. Zarko, and Z. Hanic, "A novel method for no-load magnetic field analysis of saturated surface permanent-magnet machines using conformal mapping and magnetic equivalent circuits," *IEEE Trans. Magn.*, vol. 31, no. 2, Nov. 2016, pp. 740-749, doi: 10.1109/TEC.2015.2507704.
- [15] Y. Liu, Z. Zhang, W. Geng, and J. Li, "A simplified finite-element model of hybrid excitation synchronous machines with radial/axial flux paths via magnetic equivalent circuit," *IEEE Trans. Magn.*, vol. 53, no. 11, Nov. 2017, Art. no. 7403004, doi: 10.1109/TMAG.2017.2696568.
- [16] M. Farhadian, M. Moallem, B. Fahimi, "Analytical calculation of magnetic field components in synchronous reluctance machine accounting for rotor flux barriers using combined conformal mapping and magnetic equivalent circuit methods," *Journal of Magnetism and Magnetic Materials*, vol. 505, no. 1, July 2020, 166762, <https://doi.org/10.1016/j.jmmm.2020.166762>.
- [17] L.J. Wu, Z. Li, X. Huang, Y. Zhong, Y. Fang, and Z. Q. Zhu, "A hybrid field model for open-circuit field prediction in surface-mounted PM machines considering saturation," *IEEE Trans. Magn.*, vol. 54, no. 6, June 2018, Art. no. 8103812, doi: 10.1109/TMAG.2018.2817178.
- [18] B. Nedjar, L. Vido, S. Hlioui, Y. Amara, and M. Gabsi, "Hybrid coupling: magnetic equivalent circuit coupled to finite element analysis for PMSM electromagnetic modeling," in *Proc. ISIE*, pp. 858-862, Hangzhou, China, 28-31 May 2012, doi: 10.1109/ISIE.2012.6237201.
- [19] R. Benlamine, F. Dubas, S-A. Randi, D. L. hotellier, and C. Espanet, "3-D numerical hybrid method for PM eddy-current losses calculation: Application to axial-flux PMSMs," *IEEE Trans. Magn.*, vol. 51, no. 7, July 2015, Art. no. 8106110, doi: 10.1109/TMAG.2015.2405053.
- [20] A. Demenko, J. K. Sykulski, "Analogies between Finite Difference and Finite Element Methods for Scalar and Vector Potential Formulations in Magnetic Field Calculations," *IEEE Trans. Magn.*, vol. 52, no. 6, June 2016, Art. no. 7004206, doi: 10.1109/TMAG.2016.2521345.
- [21] Q. Sun, R. Zhang, Q. Zhan, and Q. H. Liu, "3-D implicit-explicit hybrid finite difference/spectral element/finite element time domain method without a buffer zone," *IEEE Trans. Antennas Propag.*, vol. 67, no. 8, Aug. 2019, pp. 5469-5476, doi: 10.1109/TAP.2019.2913740.
- [22] Q. Sun, Q. Ren, Q. Zhan, and Q. H. Liu, "3-D domain decomposition based hybrid finite-difference time-domain/finite-element time-domain method with nonconformal meshes," *IEEE Trans. Microw. Theory Tech.*, vol. 65, no. 10, Oct. 2017, pp. 3682-3688, doi: 10.1109/TMTT.2017.2686386.
- [23] B. Yan, Y. Yang X. Wang, "A semi-numerical method to assess start and synchronization performance of a line-start permanent magnet synchronous motor equipped with hybrid rotor," *IET Elect. Power Appl.*, vol. 15, no. 4, pp. 487-500, Feb. 2021, doi: 10.1049/elp2.12043.
- [24] T. Carpi, Y. Lefèvre, and C. Henaux, "Hybrid modeling method of magnetic field of axial flux permanent magnet machine", XIII International Conference on Electrical Machines (ICEM), Greece, pp.766-772, Sep. 2018, doi: 10.1109/ICELMACH.2018.8506756.
- [25] D.C. Meeker, "Finite Element Method Magnetics", Version 4.2, 2019, Build, <http://www.femm.info>.
- [26] B. Ladghem-Chikouche, K. Boughrara, F. Dubas, and R. Ibtouen, "2-D semi-analytical magnetic field calculation for flat permanent-magnet linear machines using exact subdomain technique," *IEEE Trans. Magn.*, Early Access Article, doi: 10.1109/TMAG.2021.3068326.
- [27] F. Dubas, and K. Boughrara, "New scientific contribution on the 2-D subdomain technique in Cartesian coordinates: Taking into account of iron parts," *Math. Comput. Appl.*, vol. 22, no. 1, p. 17, Feb. 2017, doi: 10.3390/mca22010017.
- [28] L. Roubache, K. Boughrara, F. Dubas, and R. Ibtouen, "Elementary subdomain technique for magnetic field calculation in rotating electrical machines with local saturation effect," *COMPEL - Int. J. Comput. Math. Electr. Electron. Eng.*, vol. 38, no. 1, pp. 24-45, Jan. 2019, doi: 10.1108/COMPEL-11-2017-0481.



Brahim Ladghem-Chikouche was born in M'sila, Algeria, in 1981. He received the Engineer Diploma degree from the University of M'sila, M'sila, Algeria, in 2005, the Magister and the Ph.D degree from Ecole Nationale Polytechnique (ENP), Algiers, Algeria, in 2009 and 2018 respectively.

Before joining the University of M'sila in 2009, he has served in the industrial equipment maintenance sector, and electricity production company SPE-SONELGAZ, M'sila. He is currently a Lecturer at the department of Electrical Engineering, Faculty of Technology, University of M'sila, Algeria and member of the Laboratoire de Recherche en Electrotechnique (LRE-ENP), Ecole Nationale Polytechnique, Algiers, Algeria. His current research interests include electromagnetic actuation systems modeling and design.



Kamel Boughrara was born in Algiers, Algeria, in 1969. He received the Engineer Diploma degree from Ecole Nationale Polytechnique (ENP), Algiers, in 1994, the Magister degree from the University of Sciences and Technology Houari Boumediene, Algiers, in 1997, and the Ph.D. degree from ENP, in 2008. He is currently a

Professor with ENP, where he is also the head of department of Electrical Engineering.

His current research interests include the modeling and control of electrical machines.



Frédéric Dubas was born in Vesoul, France, in 1978. He received the M.Sc. degree and the Ph.D. degree from the "Univ. Bourgogne Franche-Comté" (Besançon, France) in 2002 and 2006, respectively, with a focus on the design and the optimization of high-speed surface-mounted permanent-magnet (PM)

synchronous motor for the drive of a fuel cell air-compressor. From 2014 to 2016, he has been the Head of "Unconventional Thermal and Electrical Machines" Team. He is the Head of the "Electrical Actuators" group in the "Hybrid & Fuel Cell Systems, Electrical Machines (SHARPAC)" Team. He works with ALSTOM Transports (Ornans, France), and RENAULT Technocenter (Guyancourt, France), where he is involved in the modelling, design and optimization of electrical systems and, in particular, induction and PM synchronous (radial and/or

axial flux) machines, creative problem solving, and electrical propulsion/traction. He is currently an Associate Professor with the Dép. ENERGIE, FEMTO-ST Institute affiliated to the CNRS and jointly with the “Univ. Bourgogne Franche-Comté” (Besançon, France).

He has authored over 100 refereed publications and he holds a patent about the manufacturing of axial-flux PM machines with flux-focusing. Dr. Dubas received: i) the Prize Paper Awards in the IEEE Conference Vehicle Power and Propulsion (VPPC) in 2005, ii) the Prize Presentation Awards in the 19th International Conference on Electrical Machines and Systems (ICEMS) in 2017, iii) the RENAULT Internal Award (Direction Engineering Alliance – Innovation) in 2019.



Lazhar Roubache was born in M’sila, Algeria, in 1991. He received the master’s degree and the Ph.D. degree from Ecole Nationale Polytechnique (ENP), Algiers, Algeria, in 2015 and 2019.

From 2019 to 2020, he was R&D engineer at Société d’Accélération du Transfert de Technologie Satt-Nord (Lille, France).

His current research interests include designs, modeling, optimization, and control of electrical machines.



Rachid Ibtouen received the Ph.D. degree in electrical engineering from Ecole Nationale Polytechnique (ENP), Algiers, Algeria, and the Institut National Polytechnique de Lorraine, Nancy, France, in 1993. He was with the Groupe de Recherche en Électrotechnique et Électronique de Nancy (GREEN), Nancy, from 1988 to 1993. From 2005 to 2013, he was the Director of the Laboratoire de Recherche en Electrotechnique (LRE) with ENP.

His current research interests include the modelling electric systems and drives, and, in particular, electrical machines.